

# Origin of the X-ray Induced Damage in Perovskite Solar Cells

Xuezeng Dai, *Member, IEEE*, Chengbin Fei, Praneeth Kandlakunta, *Member, IEEE*, Liang Zhao, Zhenyi Ni, Lei R. Cao, *Senior Member, IEEE*, and Jinsong Huang

**Abstract**— Perovskite solar cells (PSCs) are promising candidates for not only terrestrial but also space applications. The remarkable power-per-weight of nearly 30 W/g makes them attractive to be deployed on a spacecraft. However, the high energy radiation in outer space could damage the PSCs, making it crucial to understand their degradation mechanism. Here, we investigated the PSCs' response to X-ray radiation, and proposed that the X-ray induced damage was attributed to the displacement of I, creating lattice defects by the radiation generated secondary electrons. We verified the hypothesis by simulating the energy deposition of X-rays in PSCs and investigating the PSCs' in-situ electronic responses to the X-ray and electron beam. Furthermore, we studied the variation in spatial distribution of trap densities under X-ray radiation, which revealed that the defect abundant perovskite/PTAA interface was the most rapidly degraded site in PSCs.

**Index Terms**— damage, perovskite, solar cells, X-ray.

## I. INTRODUCTION

THE power conversion efficiency (PCE) of perovskite solar cells (PSCs) has reached 25.7%[1], which is the highest among polycrystalline thin-film photovoltaic (PV) technologies. In addition to the intriguing optoelectronic properties, including long charge carrier diffusion length, high carrier mobility, and large absorption coefficient to ultraviolet and visible light, the solution processability of perovskite materials is particularly attractive in enabling low-cost manufacturing of PSCs at high throughput. Therefore, dozens of companies in the world are dedicated to commercializing perovskite PVs. In addition to the terrestrial applications, researchers also have explored the possibility of deploying PSCs in space.[2] One advantage of PSCs for outer space applications is the potential to reach high power-per-weight values. Due to the high optical absorption coefficient, the perovskite film only needs less than 1  $\mu\text{m}$  to collect sufficient photons to reach high efficiencies. The perovskite solar cells employed on polymer substrates have accomplished an extraordinary power-per-weight of nearly 30 W/g, which is more than double that of the nearest competing solar techniques. [3, 4] Therefore, the PSCs have been launched to earth orbit to test their reliability in real space environment. Another major promising application of perovskites is radiation detection, particularly of X-rays and gamma rays. Lead halide

perovskites have high photon attenuation coefficient due to their high effective atomic number, large mobility-lifetime ( $\mu\tau$ ) product, and simple single-crystal or large area polycrystalline film growth processes.[5] Very high sensitivities, much better than that of the state-of-the-art commercial products, have been reported from both single-crystal perovskites and polycrystalline perovskites X-ray detectors[6-9]. However, the perovskite X-ray spectral detectors still need very high quality single crystals with low noise to record single photons, whereas the spectral energy resolution is quickly approaching that of the best room temperature semiconductor detectors.[9]

A fundamental understanding of the degradation of perovskite under high energy radiation is thus essential for the broader application of perovskites. Although the two main stressors for perovskite PV terrestrial applications, *i.e.*, moisture and oxygen, are avoided in space application, the high radiation environment comprising, for example X-rays, gamma-rays, protons, ions, and electrons may cause the performance degradation of PSCs in space application. Recent studies showed that the PCE of PSCs reduced by 8% ~ 36% after being exposed at earth orbits.[10-13] The apparent efficiency reduction stems from the cosmic environment in space, characterized by significant temperature fluctuation, high energy particles, and intense radiations. Although perovskites for radiation detectors usually possess sufficient radiation tolerance for low-dose radiation detection[8, 9, 14], it is not yet clear whether the perovskites can maintain their optoelectronic properties, particularly the low trap densities, under high dose irradiation.

To investigate the high dose radiation impacts, acceleration tests have been carried out.[15-18] Among them, X-ray induced degradation was often studied using radiation source from X-ray photoelectron spectroscopy (XPS). [19, 20] A decomposition of perovskites into  $\text{PbI}_2$  or metallic  $\text{Pb}^0$  was observed in these measurements. However, this might not represent the actual perovskite material response in real encapsulated solar cells, because bare perovskite films were put in a high vacuum during XPS characterization, in which the methylammonium or iodine could readily escape from the film surface. Bertoni et al. investigated the response of the PSCs to a nanosized synchrotron X-ray beam.[16] They reported that

This research project is sponsored by the Department of the Defense, Defense Threat Reduction Agency under Grant HDTRA1-19-1-0024.

Xuezeng Dai, Chengbin Fei, Liang Zhao, Zhenyi Ni, and Jinsong Huang are with Department of Applied Physical Sciences, University of North Carolina at Chapel Hill, Chapel Hill, NC 27599, USA

Praneeth Kandlakunta and Lei R. Cao are with Department of Mechanical and Aerospace Engineering, Ohio State University, Columbus, OH 43210, USA

Corresponding author: Jinsong Huang (email: jhuang@unc.edu)

an increased charge recombination contributed to the initial electronic degradation of PSCs, and the compositional change of perovskites occurred upon a high accumulated dose of X-rays. However, these studies have not elucidated how the X-rays created the charge recombination centers, *i.e.*, the origin of X-ray induced perovskite degradation. It is not clear whether the mechanism of radiation damage due to displacement of atoms that occurs in typical high energy particle interaction with the lattice bound atoms in a semiconductor is still applicable in case of perovskites.

In this study, we showed that the X-ray induced performance degradation of perovskite originates from the interaction of secondary electrons produced by X-rays, creating mobile I<sup>-</sup> ions. Our experiments revealed that the X-ray induced degradation resembled electron beam induced degradation, which was also supported by Monte Carlo simulations. The electrons produced in X-ray interaction with perovskite induced iodide interstitial defects formation in perovskites. Furthermore, we investigated the damage evolution in PSCs by characterizing the changes in spatial defect density distribution under X-ray radiation. And the degradation under X-ray radiation has been demonstrated to be different from that under light illumination.

## II. RESULTS

The investigations of X-ray induced degradation on perovskites have been usually conducted on bare films, which however, do not directly provide the response information of PSC devices under X-ray irradiation. The device performance could substantially change by a minor amount of defect density change, which is usually at the level of parts per million or less, before the apparent material composition or morphology change is observed on the bare films. In addition, the interfaces and other functional layers, such as hole/electron transporting layers, could also be directly or indirectly damaged by X-rays, which profoundly impacts charge collection. Therefore, instead of bare films, we tracked the output electric signal from a full assembled PSC in response to X-ray radiation. To that end, we designed an *in-situ* X-ray measurement setup as shown in **Fig. 1a** (**Fig. S1**). The X-ray source (iVario-225/2.25, COMET) generated high intensity X-rays with a dose rate of 450 mGy/s (measured in air by a dosimeter; X-ray tube: 120 kV, 3 mA) on a large area of around 10 cm<sup>2</sup>. The incident angle of X-ray was set to be 45° with respect to the PSC's surface. To mimic the working condition of an operating PSC, a light source illuminated visible light on PSCs with an incident angle of 45°. For the perovskite solar devices, we leveraged our demonstrated scalable coating technique to fabricate perovskite solar minimodules, which had a much larger photovoltaic output than single cells.<sup>[21]</sup> The device material stack and a typical *IV* curve are shown in **Fig. S2**. The perovskite solar minimodule contained several subcells connected in series, resulting in a high photovoltaic output. We recorded the photovoltaic output from the solar minimodules using a source meter (2400, Keithley). After the photovoltaic output from the PSCs stabilized, the X-ray source was turned on to bombard the PSCs with X-rays for 30 s, and then turned off.

**Figures 1b and 1c** demonstrate PSC's responses to X-ray

radiation under 1 Sun and 0.05 Sun illuminations, respectively. Here 1 Sun light intensity is equivalent to 100 mW/cm<sup>2</sup>. Two different light intensities were selected to investigate the PSCs' responses under different device temperatures and free carrier densities, which might impact the device response dynamics. The photovoltaic declined instantly under X-ray radiation regardless of the visible light intensities, indicating the presence of electronic damage on PSCs by X-rays. However, the photovoltaic slowly recovered after turning off the X-ray, which can be explained by the broadly observed self-healing feature of metal halide perovskite materials.<sup>[22, 23]</sup> The self-healing attributes to the annihilation of the trap states, for example, the filling of iodine vacancies by iodine interstitials, or the conversion of positively and negatively charged iodine interstitials into iodine.<sup>[24]</sup> The self-healing dynamics are sensitive to the device temperature and light intensity, where a higher temperature could accelerate the recovery because of the fast ion migration.<sup>[23, 25]</sup> This agrees with the experiment results shown in **Fig. 1b and 1c** that 1 Sun illumination, which induced a higher device temperature and faster ion migration, triggered a faster recovery than 0.05 Sun illumination. It is noted that a high light intensity also causes degradation of perovskite solar cells, but that generally occurs at a much longer duration.<sup>[23]</sup>

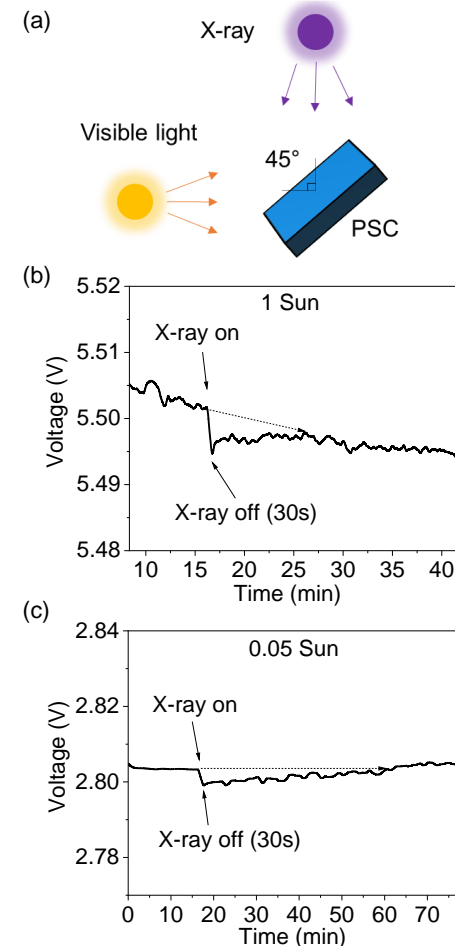


**Fig. 1. In-situ study of perovskite solar cell output change under X-ray radiation.** (a) The in-situ measurement setup of perovskite solar device response to X-ray radiation. (b, c) The photovoltaic output under X-ray radiation with different background light intensities of (b) 1 Sun, (c) 0.05 Sun.

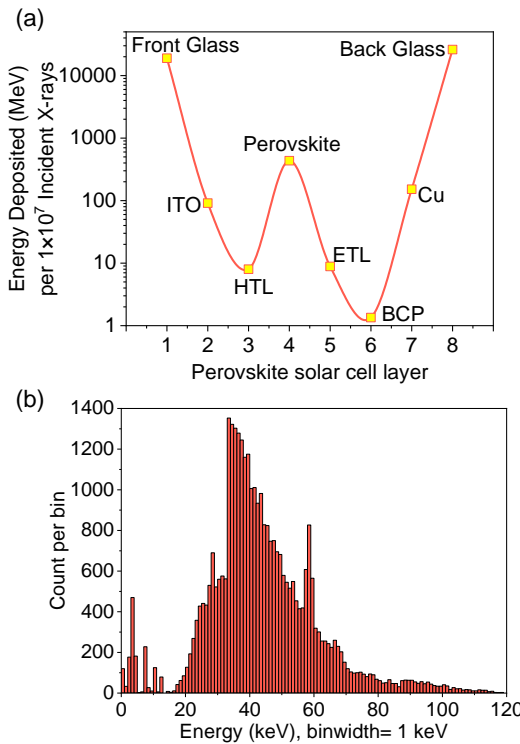


**Fig. 2. The simulation of energy deposition in perovskite solar cells.** (a) The energy deposition from 120 kV X-rays in different material layers of perovskite solar cells. (b) The energy spectrum of photoelectrons generated by the 120 kV X-rays in the perovskite layer.

To understand the amount of energy deposited in each layer of PSC from the 120 kV X-rays and gain insights into the mechanism of X-ray induced damage in PSCs, we performed Monte Carlo (MC) simulations in Geant4[26]. In the MC simulations, a photon disk source was used, which emitted X-rays with an energy distribution matching the spectrum of 120 kV X-rays produced by the X-ray tube (iVario-225/2.25, COMET). The X-rays were orthogonally incident on the front glass layer (i.e., the bottommost layer) of the PSC material stack shown in **Fig. S2(a)**. The total energy deposited in each material layer from the interaction of 120 kV X-rays with PSC was calculated in Geant4, which considered the energy deposited by all the energy loss processes, while accounting for the transport of all secondary particles, including that of secondary electrons through different PSC material layers. The simulation result of energy deposition from 120 kV X-rays in different material layers of PSC is shown in **Fig. 2a**, which indicates that the X-ray energy was mainly deposited into the glasses and the perovskite layer. The high dose accumulated in glass could produce structural defects, which generate new absorption bands that darken the glass.[15] Similarly, a portion of the total dose deposited in perovskite layer could also lead to defects in the perovskite lattice structure, leading to the output voltage drop as shown in **Fig. 1b and 1c**. However, since the electromagnetic radiation such as X-rays, do not directly interact with the nucleus to cause atom displacement,[27] the secondary photoelectric electrons and Compton electrons, generated by the intense X-rays were considered to be the source producing defects in perovskites. The electron-induced damage in perovskite materials has been reported since

2015.[28] High dose electrons could lead to phase transformation or decomposition of perovskites.[29, 30] The electron beam driven ion migration has been directly observed by transmission electron microscopy (TEM) study.[17]

Here we calculated the threshold energy ( $E$ ) the electrons need to displace atoms from their lattice by:[27]

$$E_a = \frac{2E(E + mc^2)}{Mc^2} \quad (1)$$

where  $E_a$  is the activation energy of the atom,  $m$  is the electron mass,  $M$  is the atom mass, and  $c$  is the speed of light. In hybrid halide perovskites, the activation energies of the organic cations and  $\text{Pb}^{2+}$  were roughly around 0.8 eV and 2.3 eV, whereas the activation energy of  $\text{I}^-$  was reported to be in the range of 0.08 eV to 0.62 eV.[31, 32] According to equation (1), the corresponding threshold electron energies to cause their displacements are about 12 keV, 185 keV, and a range of 4.6 keV to 34.6 keV, respectively. Meanwhile, the energy distribution of the photoelectrons generated by 120 kV X-rays in the perovskite layer has been simulated in Geant4. **Fig. 2b** shows that photoelectrons are mainly distributed in 20 keV to 80 keV, which is sufficiently higher than the threshold electron energies to activate the organic cations and  $\text{I}^-$  in perovskite. Our previous work has demonstrated that the excess charges, either generated by incident light or external electrical injections, could reduce the activation energy for ion migration within perovskites, accelerating the degradation when the density of electrons is very high.[25] Therefore, the high energy excess charges generated by X-ray radiation, which accumulated in the device in a short time, most possibly facilitated the defects formation that degraded the device photovoltaic performance.

To verify that X-ray induced damage arose from the radiation generated electrons, we directly used electron beams to irradiate the PSCs and compared the photovoltaic responses with that caused by X-ray radiation. As shown in **Fig. 3a**, an electron beam (e-beam) was generated from a scanning electron microscopy (SEM, FEI Helios 600 Nanolab) system, in which the maximum diameter of the electron beam was 1.9 mm. To induce sufficient electron impact, a small area perovskite solar cell (2 mm  $\times$  4 mm) comparable to the electron beam size was used in this test. A light emitting device was used to illuminate visible light onto the target PSC. As these low energy electrons cannot penetrate the 0.7 mm glass encapsulation of perovskite solar devices, the glass layer was removed in the small area PSC such that the electron beam entered the perovskites through the thin Cu electrode of the PSC. And the Cu thickness was reduced to 20 nm to reduce the energy loss electrons in Cu. To understand the penetration depth, we simulated the bombardment of 2 keV, 5 keV, and 10 keV e-beams (86 pA current) onto this PSC using CASINO v2.51 software[33]. The result in **Fig. 3c-3e** revealed that the 2 keV e-beam could barely penetrate the top Cu layer, whereas half of the 5 keV e-beam reached the perovskite layer, and most of the 10 keV e-beam penetrated into the perovskite layer. The corresponding photovoltaic responses to the e-beam bombardments are shown in **Fig. 3b**. There was no reduction in photovoltaic with the 2 keV e-beam irradiation, which was attributed to the electrons

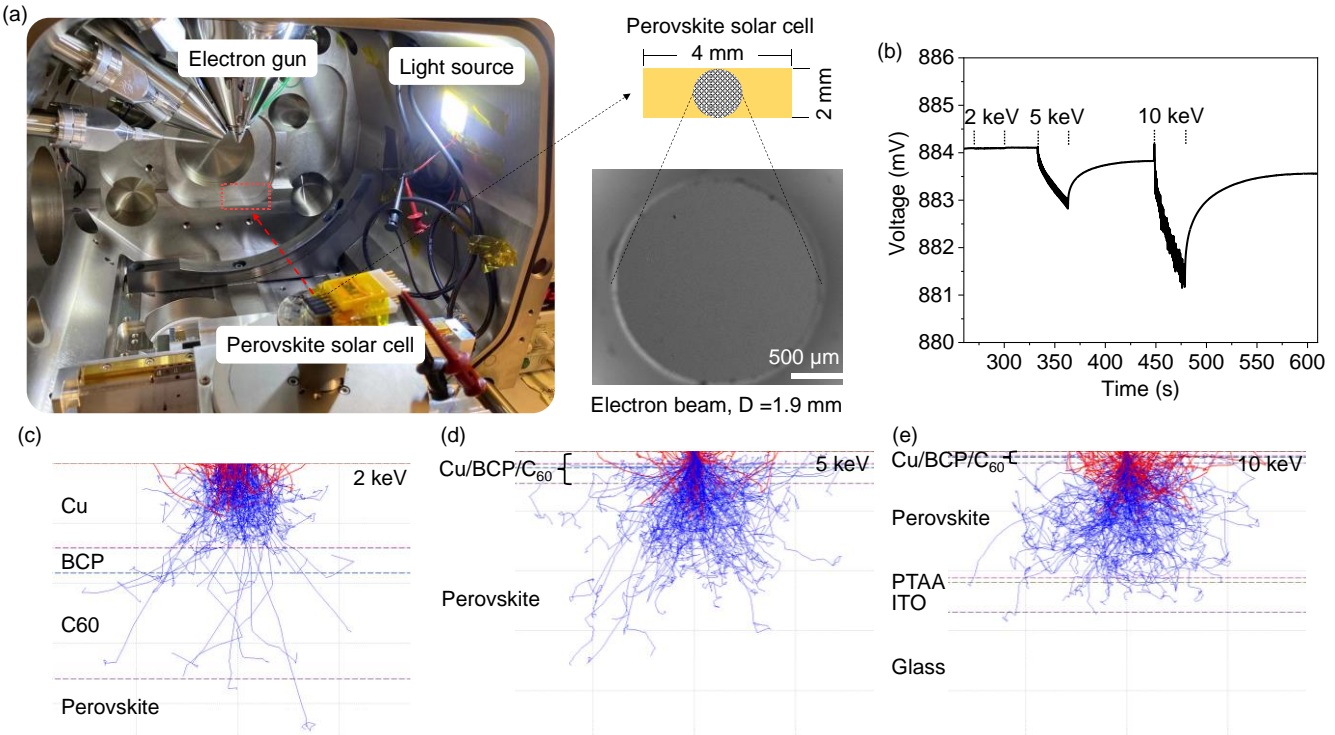


**Fig. 3 In-situ electron-beam radiation reaction on perovskite solar devices.** (a) The in-situ measurement setup of perovskite solar device response to electron beam. (b) The electric signal response under electron beam. (c-e) The simulation of electron beam penetration in perovskite solar cells for electron energies- (c) 2 keV, (d) 5 keV, (e) 10 keV.

not reaching the perovskite layer and the energy was insufficient to cause ion movements in perovskite. On the contrary, the photovoltage decreased when the 5 keV e-beam bombarded the PSC and entered perovskite layer, and the drop in voltage was even higher when the 10 keV e-beam penetrated through the whole perovskite layer. Both the 5 keV and 10 keV electron energies were higher than the threshold to displace the I<sup>-</sup> (minimum value: 4.6 keV), consequently, creating lattice defects that reduced PSC's photovoltaic performance. Nevertheless, the reduced photovoltage slowly recovered after shutting the e-beam off, which is attributed to the self-healing effect explained above. The similar responses from e-beam and X-ray irradiations verified that the X-ray induced radiation damage of PSCs originated indeed from those secondary electrons produced by X-rays.

Furthermore, we investigated the dynamics of evolution of the X-ray induced degradation in the perovskite devices. We characterized the trap density changes of a small area PSC (8 mm<sup>2</sup>) that was irradiated under the same setup in **Fig. 1**, where 450 mGy/s X-rays irradiated from the PTAA side of PSC through a glass of 0.7 mm. First, we monitored the trap density of states (tDOS) change in perovskite film by the thermal admittance spectroscopy (TAS) method. The energy dependent tDOS are shown in **Fig. 4a**, where three energy bands can be identified. Our recent work had verified that the traps in energy band I were mainly attributed to the negative iodide interstitial (I<sub>i</sub><sup>-</sup>); the traps in energy band II stemmed from the positive iodide interstitial (I<sub>i</sub><sup>+</sup>); and the traps in energy band III was speculated as lead vacancies (V<sub>Pb</sub>). **Fig. 4a** demonstrates

that 60 min (250 Gy) of X-ray radiation increased the I<sub>i</sub><sup>-</sup> density but reduced the I<sub>i</sub><sup>+</sup> density in PSCs.

To further understand the evolution of defects in perovskite film, we characterized the spatial distributions of the trap states via the drive-level capacitance profiling (DLCP) method.[34] Our previous work has demonstrated that the DLCP is a feasible technique to profile both the spatial and energy distribution of defects in PSCs.[24] The position of trap states in real space was detected by tuning the direct current (DC) bias applied to the depletion region of the junctions. The energy distribution was extracted by adjusting the alternating current (AC) frequency applied alongside the DC bias. Any traps with energy depth shallower than a critical value could respond to the AC frequency and contribute to the total carrier density. The lower the applied AC frequency, the deeper the trap states could be detected. The trap density of a certain energy range can be estimated by subtracting the total carrier density measured at high AC frequency from that measured at low AC frequency. For the profiling distance, the 0 distance side on DLCP figures has been identified as the C<sub>60</sub>/perovskite interface, which resembles as an n<sup>+</sup>-p junction.[34] We characterized the carrier densities of 1000 kHz (0.23 eV), 100 kHz (0.29 eV), and 10 kHz (0.35 eV) from the pristine PSC and the device after being irradiated for 30 min (90 Gy) and 60 min (250 Gy), respectively (**Fig. S3 a-c**). Then the trap densities mainly located in Band I and Band II could be extracted by subtracting the densities measured from the energy depth of 0.23 eV from 0.29 eV, and energy depth of 0.29 eV from 0.35 eV, respectively.

As a result, the change in I<sub>i</sub><sup>-</sup> defects at Band I and that in I<sub>i</sub><sup>+</sup> defects at Band II are shown in **Fig. 4b and 4c**, which demonstrated that I<sub>i</sub><sup>-</sup> and I<sub>i</sub><sup>+</sup> defect changes varied through the

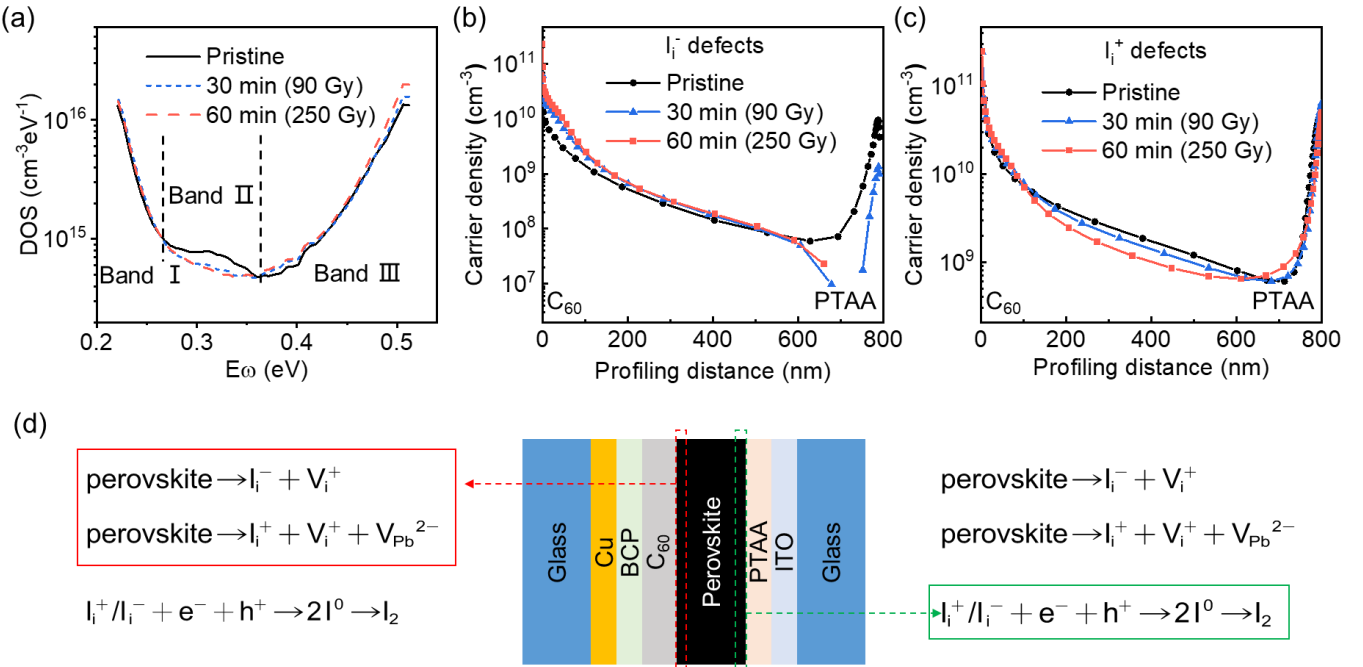


**Fig. 4** The defects evolution in perovskite solar cells under X-ray radiation. (a) tDOS spectra of perovskite solar cells evolved under X-ray radiation. (b, c) spatial distributions of  $\text{I}_i^-$  and  $\text{I}_i^+$  defects evolved under X-ray radiation. (d) Schematic of the damage evolution in the perovskite solar cells.

film within 60 min of irradiation (250 Gy). Under irradiation, both  $\text{I}_i^-$  and  $\text{I}_i^+$  densities near  $\text{C}_{60}$ /perovskite interface increased, which agreed with our previous investigation of defect evolutions under long-term light illumination (Fig. S4).[24] On the contrary, both  $\text{I}_i^-$  and  $\text{I}_i^+$  densities subsided near PTAA/perovskite interface, which was different from light induced degradation that had  $\text{I}_i^-$  density reduced but  $\text{I}_i^+$  density increased. We conducted the characterization on another cell but with the same perovskite composition. The result in Fig. S5 shows the same shifting of  $\text{I}_i^-$  and  $\text{I}_i^+$  defect densities on the two interfaces under X-ray radiation, which confirms the reliability of the defect density changing. Under light illumination, the opposite change of  $\text{I}_i^-$  and  $\text{I}_i^+$  defect densities near PTAA/perovskite interface was attributed to the light induced defect-annihilation reaction, in which the recombination of  $\text{I}_i^-$  and  $\text{V}_i^+$  consumed the density of  $\text{I}_i^-$  but left  $\text{I}_i^+$  piling up.[24, 35] For X-ray radiation, however, the reduction of both defects could be because the perovskite near PTAA had already entered a decomposition phase, during which the detected  $\text{I}_i^+$  and  $\text{I}_i^-$  started to decrease. As the perovskite close to the PTAA side was originally the most defect dense[21], it was much easy to completely convert to  $\text{I}_i^+$  and  $\text{I}_i^-$  defects under the intense X-ray radiation. Then the saturated defects trapped the photogenerated electrons and holes, which formed  $\text{I}_2$  that was released from the lattice and thus, the concentration of these defects (Fig. 4d) was reduced. And the fast decomposition in short time prohibited the defect-annihilation effect near the PTAA/perovskite interface. In the bulk of the perovskite film, the enhancement of  $\text{I}_i^-$  defect density and weakening of  $\text{I}_i^+$  defect density under X-ray radiation represented the competition between the loss of defects from decomposition and the generation of defects from intact perovskites. But in

commercial solar panels, the much thicker glass of  $\sim 5$  mm[36, 37] could dramatically attenuate the X-ray intensity and alter the degradation dynamics more similar to those under long-duration light illumination.

### III. CONCLUSION

The X-ray induced damage on perovskite solar cells has been shown to originate from the interaction of energetic electrons produced by X-ray radiation. The X-ray induced electrons were shown to increase the defect densities that lowered the PSCs performance. In addition, the degradation pathway in PSCs has been investigated. The X-rays triggered a rapid decomposition at the PTAA/perovskite interface, where the defects were originally abundant. Our investigation showed that passivating the defects at perovskite interfaces or improving the charge extraction from the perovskite film could improve the stability of PSCs under X-ray radiations.

### IV. METHODS

#### A. Fabrication of perovskite solar devices

Patterned ITO glass substrates were cleaned by ultrasonication with soap, deionized water, and isopropyl alcohol, and then UV-ozone treated for 15 min before use. All perovskite solar devices were prepared by blade-coating at room temperature inside a fume hood. The hole-transporting PTAA layer with a concentration of  $3.3 \text{ mg} \cdot \text{mL}^{-1}$  dissolved in toluene was blade-coated onto ITO glass substrates at a speed of  $20 \text{ mm} \cdot \text{s}^{-1}$  in ambient air ( $20 \pm 1^\circ \text{C}$ ,  $30 \pm 5 \text{ RH\%}$ ). The perovskite precursor solutions composed of mixed cations (lead (Pb), cesium (Cs), formamidine (FA)) and halides (I, Br) was dissolved in 2-methoxyethanol (2-ME) with a chemical formula of  $\text{Cs}_{0.1}\text{FA}_{0.9}\text{PbI}_3$ . Before blade-coating, 70 mol% dimethyl

sulfoxide (DMSO) with respect to Pb was added to the target perovskite precursor solution. Subsequently, the precursor solution was blade-coated onto the PTAA-covered ITO glass substrates at a blading speed of 20 mm s<sup>-1</sup> in ambient air (20 ± 1 °C, 30 ± 5 RH%). After that, the perovskite films were annealed at 150 °C for 3 min in air. The solar cells were completed by thermally evaporating C60 (30 nm), BCP (6 nm), and copper (100 nm). The solar module was encapsulated in ambient air with epoxy and glass on top.

### B. Characterization

The X-ray irradiation tests were conducted in ambient air. An X-ray source (iVario-225/2.25, COMET) was set at 120 kV and 3 mA, which generated high intensity X-rays with a dose rate of 450 mGy/s on an area of around 10 cm<sup>2</sup>. A projector (BenQ MX720) projecting white light was used to illuminate visible light onto the PSCs. The light intensity was measured by a silicon reference cell with a KG5 glass filter (Newport 91150 V). The incident angles of X-ray and visible light were both set to be 45° with respect to the PTAA side of PSCs. The photovoltage was tracked by a source meter (2400, Keithley). The environment had a temperature of 20 ± 1 °C with a humidity of 30 ± 5 RH%. The perovskite module aperture area was 8.25 cm<sup>2</sup>.

The e-beam tests were conducted in a scanning electron microscopy (SEM) chamber. The e-beam was generated from the electron gun of SEM (FEI Helios 600 Nanolab), with a maximum diameter of 1.9 mm. An LED light (12V, YM E-Bright) was attached on the SEM chamber to illuminate visible light onto PSCs. The photovoltage was recorded by a source meter (2400, Keithley) connected to the BNC feedthrough connectors on the SEM chamber. The environment temperature was 20 ± 1 °C. The active area of small PSC was 8 mm<sup>2</sup>. The electron beam voltage was tuned within 2 kV, 5 kV, and 10 kV with a current of 8.6 pA.

The TAS and DLCP were characterized using an LCR meter (Agilent E4989A). For TAS measurement, the DC bias and the amplitude of AC bias were 0 V and 20 mV, respectively. The frequency was scanned from 0.02 kHz to 2000 kHz. The DLCP measurement was scanned from 0 V to the  $V_{OC}$  of the PSCs. The environment had a temperature of 20 ± 1 °C with a humidity of 30 ± 5 RH%. More detail of the TAS and DLCP measurements are described in our previous work.[24]

## V. ACKNOWLEDGMENTS

### A. Funding

This work was mainly supported by Defense Threat Reduction Agency under grant HDTRA1-19-1-0024. The content of the information does not necessarily reflect the position or the policy of the federal government, and no official endorsement should be inferred.

### B. Competing interests

Authors declare that they have no competing interests.

### C. Data and materials availability

All data needed to evaluate the conclusions in the paper are

present in the paper and/or the Supplementary Materials. Additional data related to this paper may be requested from J.H. (jhuang@unc.edu).

## REFERENCES

- [1] NREL. "Best Research-Cell Efficiency Chart." [www.nrel.gov/pv/cell-efficiency.html](http://www.nrel.gov/pv/cell-efficiency.html) (accessed February 11, 2022).
- [2] Y. Tu, J. Wu, G. Xu, X. Yang, R. Cai, Q. Gong, R. Zhu, and W. Huang, "Perovskite solar cells for space applications: progress and challenges," *Adv. Mater.*, vol. 33, no. 21, Apr. 2021, Art No. 2006545, doi: 10.1002/adma.202006545.
- [3] Y. Hu, T. Niu, Y. Liu, Y. Zhou, Y. Xia, C. Ran, Z. Wu, L. Song, P. Müller-Buschbaum, and Y. Chen, "Flexible perovskite solar cells with high power-per-weight: progress, application, and perspectives," *ACS Energy Lett.*, vol. 6, no. 8, pp. 2917-2943, Jul. 2021, doi: 10.1021/acsenergylett.1c01193.
- [4] S. Kang, J. Jeong, S. Cho, Y. J. Yoon, S. Park, S. Lim, J. Y. Kim, and H. Ko, "Ultrathin, lightweight and flexible perovskite solar cells with an excellent power-per-weight performance," *Journal of Materials Chemistry A*, vol. 7, no. 3, pp. 1107-1114, Dec. 2018, doi: 10.1039/C8TA10585E.
- [5] H. Wei and J. Huang, "Halide lead perovskites for ionizing radiation detection," *Nature communications*, vol. 10, no. 1, Mar. 2019, Art No. 1066, doi: 10.1038/s41467-019-08981-w.
- [6] S. Deumel, A. van Breemen, G. Gelinck, B. Peeters, J. Maas, R. Verbeek, S. Shannugam, E. Akkerman, E. Meulenkamp, and J. E. Huerdler, "High-sensitivity high-resolution X-ray imaging with soft-sintered metal halide perovskites," *Nature Electronics*, vol. 4, no. 9, pp. 681-688, Sep. 2021, doi: 10.1038/s41928-021-00644-3.
- [7] H. Wei, Y. Fang, P. Mulligan, W. Chuirazzi, H.-H. Fang, C. Wang, B. R. Ecker, Y. Gao, M. A. Loi, and L. Cao, "Sensitive X-ray detectors made of methylammonium lead tribromide perovskite single crystals," *Nat. Photonics*, vol. 10, no. 5, pp. 333-339, Mar. 2016, doi: 10.1038/nphoton.2016.41.
- [8] J. Zhao, L. Zhao, Y. Deng, X. Xiao, Z. Ni, S. Xu, and J. Huang, "Perovskite-filled membranes for flexible and large-area direct-conversion X-ray detector arrays," *Nat. Photonics*, vol. 14, no. 10, pp. 612-617, Aug. 2020, doi: 10.1038/s41566-020-0678-x.
- [9] Y. Zhou, L. Zhao, Z. Ni, S. Xu, J. Zhao, X. Xiao, and J. Huang, "Heterojunction structures for reduced noise in large-area and sensitive perovskite x-ray detectors," *Sci. Adv.*, vol. 7, no. 36, pp. eabg6716, Sep. 2021, doi: 10.1126/sciadv.abg6716.
- [10] Y. Miyazawa, M. Ikegami, H.-W. Chen, T. Ohshima, M. Imaizumi, K. Hirose, and T. Miyasaka, "Tolerance of perovskite solar cell to high-energy particle irradiations in space environment," *IScience*, vol. 2, pp. 148-155, Apr. 2018, doi: 10.1016/j.isci.2018.03.020.
- [11] L. K. Reb, M. Böhmer, B. Predeschly, S. Grott, C. L. Weindl, G. I. Ivandekic, R. Guo, C. Dreißigacker, R. Gernhäuser, and A. Meyer, "Perovskite and organic solar cells on a rocket flight," *Joule*, vol. 4, no. 9, pp. 1880-1892, Sep. 2020, doi: 10.1016/j.joule.2020.07.004.
- [12] I. Cardinaletti, T. Vangerven, S. Nagels, R. Cornelissen, D. Schreurs, J. Hruby, J. Vodnik, D. Devisscher, J. Kesters, and J. D'Haen, "Organic and perovskite solar cells for space applications," *Sol. Energy Mater. Sol. Cells*, vol. 182, pp. 121-127, Aug. 2018, doi: 10.1016/j.solmat.2018.03.024.
- [13] Y. Tu, G. Xu, X. Yang, Y. Zhang, Z. Li, R. Su, D. Luo, W. Yang, Y. Miao, R. Cai, L. Jiang, X. Du, Y. Yang, Q. Liu, Y. Gao, S. Zhao, W. Huang, Q. Gong, and R. Zhu, "Mixed-cation perovskite solar cells in space," *Science China Physics, Mechanics & Astronomy*, vol. 62, no. 7, pp. 974221, Feb. 2019, doi: 10.1007/s11433-019-9356-1.
- [14] Q. Chen, J. Wu, X. Ou, B. Huang, J. Almutlaq, A. A. Zhumekenov, X. Guan, S. Han, L. Liang, and Z. Yi, "All-inorganic perovskite nanocrystal scintillators," *Nature*, vol. 561, no. 7721, pp. 88-93, Aug. 2018, doi: 10.1038/s41586-018-0451-1.
- [15] S. Yang, Z. Xu, S. Xue, P. Kandlakunta, L. Cao, and J. Huang, "Organohalide Lead Perovskites: More Stable than Glass under Gamma - Ray Radiation," *Adv. Mater.*, vol. 31, no. 4, pp. 1805547, Nov. 2019, doi: 10.1002/adma.201805547.
- [16] M. E. Stuckelberger, T. Nietzold, B. M. West, Y. Luo, X. Li, J. Werner, B. r. Niesen, C. Ballif, V. Rose, and D. P. Fenning, "Effects of X-rays on

perovskite solar cells," *The Journal of Physical Chemistry C*, vol. 124, no. 33, pp. 17949-17956, Jul. 2020, doi: 10.1021/acs.jpcc.0c04645.

[17] S. Chen, X. Zhang, J. Zhao, Y. Zhang, G. Kong, Q. Li, N. Li, Y. Yu, N. Xu, and J. Zhang, "Atomic scale insights into structure instability and decomposition pathway of methylammonium lead iodide perovskite," *Nature communications*, vol. 9, no. 1, pp. 1-8, Nov. 2018, doi: 10.1038/s41467-018-07177-y.

[18] F. Lang, N. H. Nickel, J. Bundesmann, S. Seidel, A. Denker, S. Albrecht, V. V. Brus, J. Rappich, B. Rech, and G. Landi, "Radiation hardness and self - healing of perovskite solar cells," *Adv. Mater.*, vol. 28, no. 39, pp. 8726-8731, Aug. 2016, doi: 10.1002/adma.201603326.

[19] K. Motoki, Y. Miyazawa, D. Kobayashi, M. Ikegami, T. Miyasaka, T. Yamamoto, and K. Hirose, "Degradation of CH<sub>3</sub>NH<sub>3</sub>PbI<sub>3</sub> perovskite due to soft x-ray irradiation as analyzed by an x-ray photoelectron spectroscopy time-dependent measurement method," *J. Appl. Phys.*, vol. 121, no. 8, pp. 085501, Feb. 2017, doi: doi.org/10.1063/1.4977238.

[20] W.-C. Lin, W.-C. Lo, J.-X. Li, Y.-K. Wang, J.-F. Tang, and Z.-Y. Fong, "In situ XPS investigation of the X-ray-triggered decomposition of perovskites in ultrahigh vacuum condition," *npj Materials Degradation*, vol. 5, no. 1, Apr. 2021, Art No. 13, doi: 10.1038/s41529-021-00162-9.

[21] S. Chen, X. Dai, S. Xu, H. Jiao, L. Zhao, and J. Huang, "Stabilizing perovskite-substrate interfaces for high-performance perovskite modules," *Science*, vol. 373, no. 6557, pp. 902-907, Aug. 2021, doi: 10.1126/science.abi6323.

[22] Y. Yu, F. Zhang, and H. Yu, "Self-healing perovskite solar cells," *Solar Energy*, vol. 209, pp. 408-414, Oct. 2020, doi: 10.1016/j.solener.2020.09.018.

[23] W. Nie, J.-C. Blancon, A. J. Neukirch, K. Appavoo, H. Tsai, M. Chhowalla, M. A. Alam, M. Y. Sfeir, C. Katan, and J. Even, "Light-activated photocurrent degradation and self-healing in perovskite solar cells," *Nature communications*, vol. 7, no. 1, May. 2016, Art No. 11574, doi: 10.1038/ncomms11574.

[24] Z. Ni, H. Jiao, C. Fei, H. Gu, S. Xu, Z. Yu, G. Yang, Y. Deng, Q. Jiang, and Y. Liu, "Evolution of defects during the degradation of metal halide perovskite solar cells under reverse bias and illumination," *Nat. Energy*, vol. 7, no. 1, pp. 65-73, Dec. 2021, doi: doi.org/10.1038/s41560-021-00949-9.

[25] Y. Lin, B. Chen, Y. Fang, J. Zhao, C. Bao, Z. Yu, Y. Deng, P. N. Rudd, Y. Yan, and Y. Yuan, "Excess charge-carrier induced instability of hybrid perovskites," *Nature communications*, vol. 9, no. 1, Nov. 2018, Art No. 4981, doi: 10.1038/s41467-018-07438-w.

[26] S. Agostinelli, J. Allison, K. a. Amako, J. Apostolakis, H. Araujo, P. Arce, M. Asai, D. Axen, S. Banerjee, and G. Barrand, "GEANT4—a simulation toolkit," *Nuclear instruments and methods in physics research section A: Accelerators, Spectrometers, Detectors, and Associated Equipment*, vol. 506, no. 3, pp. 250-303, 2003, doi: 10.1016/S0168-9002(03)01368-8.

[27] G. Kinchin and R. Pease, "The displacement of atoms in solids by radiation," *Rep. Prog. Phys.*, vol. 18, no. 1, pp. 1-51, Jan. 1955, doi: 10.1088/0034-4885/18/1/301.

[28] Y. Miyazawa, M. Ikegami, T. Miyasaka, T. Ohshima, M. Imaizumi, and K. Hirose, "Evaluation of radiation tolerance of perovskite solar cell for use in space," in *2015 IEEE 42nd Photovoltaic Specialist Conference (PVSC)*, Jun. 2015: IEEE, pp. 1178-1181, doi: 10.1109/PVSC.2015.7355859.

[29] C. Xiao, Z. Li, H. Guthrey, J. Moseley, Y. Yang, S. Wozny, H. Moutinho, B. To, J. J. Berry, and B. Gorman, "Mechanisms of electron-beam-induced damage in perovskite thin films revealed by cathodoluminescence spectroscopy," *The Journal of Physical Chemistry C*, vol. 119, no. 48, pp. 26904-26911, Nov. 2015, doi: 10.1021/acs.jpcc.5b09698.

[30] A. R. Milosavljević, W. Huang, S. Sadhu, and S. Ptasinska, "Low - energy electron - induced transformations in organolead halide perovskite," *Angew. Chem. Int. Ed.*, vol. 55, no. 34, pp. 10083-10087, Jun. 2016, doi: 10.1002/anie.201605013.

[31] C. Eames, J. M. Frost, P. R. Barnes, B. C. O'regan, A. Walsh, and M. S. Islam, "Ionic transport in hybrid lead iodide perovskite solar cells," *Nature communications*, vol. 6, no. 1, Jun. 2015, Art No. 7497, doi: 10.1038/ncomms8497.

[32] D. W. Ferdani, S. R. Pering, D. Ghosh, P. Kubiak, A. B. Walker, S. E. Lewis, A. L. Johnson, P. J. Baker, M. S. Islam, and P. J. Cameron, "Partial cation substitution reduces iodide ion transport in lead iodide perovskite solar cells," *Energ Environ. Sci.*, vol. 12, no. 7, pp. 2264-2272, May. 2019, doi: 10.1039/C9EE00476A.

[33] D. Drouin, A. R. Couture, D. Joly, X. Tastet, V. Aimez, and R. Gauvin, "CASINO V2. 42—a fast and easy - to - use modeling tool for scanning electron microscopy and microanalysis users," *Scanning: The Journal of Scanning Microscopies*, vol. 29, no. 3, pp. 92-101, 2007, doi: 10.1002/sca.20000.

[34] Z. Ni, C. Bao, Y. Liu, Q. Jiang, W.-Q. Wu, S. Chen, X. Dai, B. Chen, B. Hartweg, and Z. Yu, "Resolving spatial and energetic distributions of trap states in metal halide perovskite solar cells," *Science*, vol. 367, no. 6484, pp. 1352-1358, Mar. 2020, doi: 10.1126/science.aba0893.

[35] S. G. Motti, D. Meggiolaro, A. J. Barker, E. Mosconi, C. A. R. Perini, J. M. Ball, M. Gandini, M. Kim, F. De Angelis, and A. Petrozza, "Controlling competing photochemical reactions stabilizes perovskite solar cells," *Nat. Photonics*, vol. 13, no. 8, pp. 532-539, May. 2019, doi: 10.1038/s41566-019-0435-1.

[36] S. Jalaly, M. Vahdani, M. Shahabadi, and G. M. M. Sadeghi, "Design, fabrication, and measurement of a polymer-based anti-reflection coating for improved performance of a solar panel under a specific incident angle," *Sol. Energy Mater. Sol. Cells*, vol. 189, pp. 175-180, Jan. 2019, doi: 10.1016/j.solmat.2018.10.001.

[37] A. M. Manokar, D. P. Winston, J. D. Mondol, R. Sathyamurthy, A. Kabeel, and H. Panchal, "Comparative study of an inclined solar panel basin solar still in passive and active mode," *Solar Energy*, vol. 169, pp. 206-216, Jul. 2018, doi: 10.1016/j.solener.2018.04.060.

## Supplementary information

### Origin of the X-ray Induced Damage in Perovskite Solar Cells

Xuezeng Dai<sup>1</sup>, Chengbin Fei<sup>1</sup>, Praneeth Kandlakunta<sup>2</sup>, Liang Zhao<sup>1</sup>, Zhenyi Ni<sup>1</sup>, Lei R. Cao<sup>2</sup>, Jinsong Huang<sup>1,3\*</sup>

<sup>1</sup> Department of Applied Physical Sciences, University of North Carolina at Chapel Hill, Chapel Hill, NC 27599, USA

<sup>2</sup> Department of Mechanical and Aerospace Engineering, Ohio State University, Columbus, OH 43210, USA

<sup>3</sup> Department of Chemistry, University of North Carolina at Chapel Hill, Chapel Hill, NC 27599, USA

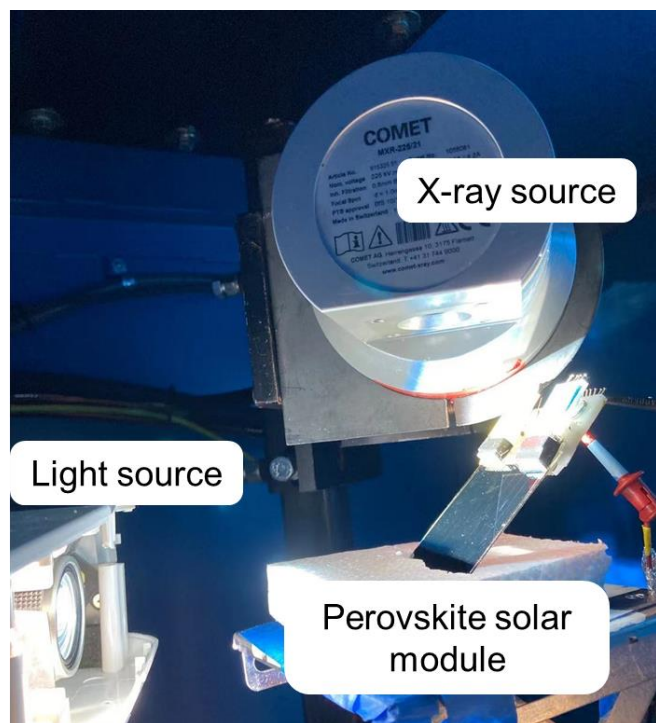


**Fig. S1.** Picture of the equipment setup of in-situ measurement on perovskite solar device response to X-ray radiation.

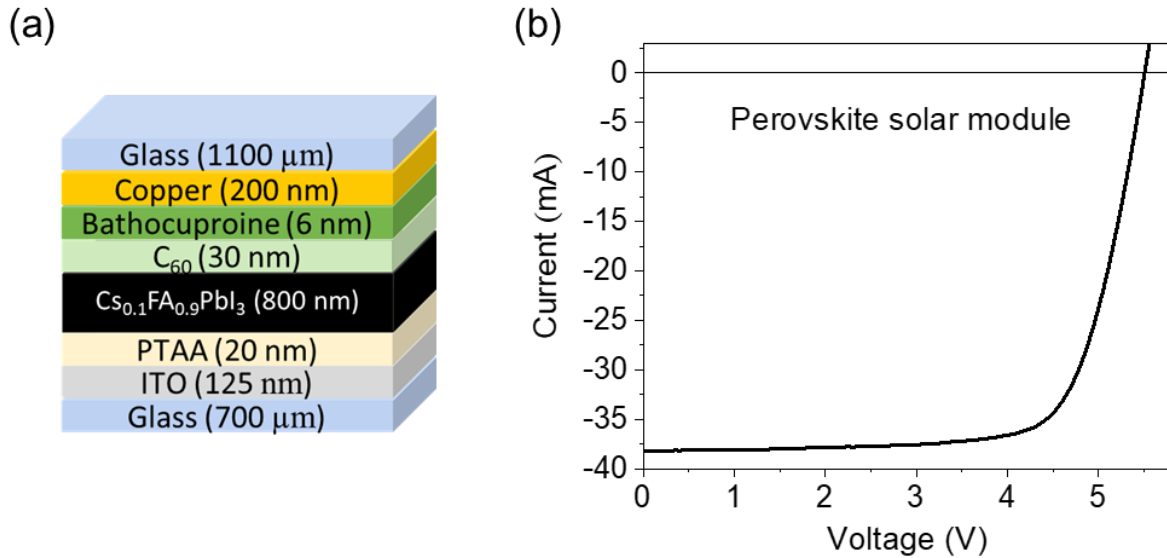


**Fig. S2.** Perovskite solar devices. (A) The material stack of perovskite solar devices used in this study. (B) A typical IV curve of the perovskite solar modules (5 subcells, aperture area  $8.25 \text{ cm}^2$ ).

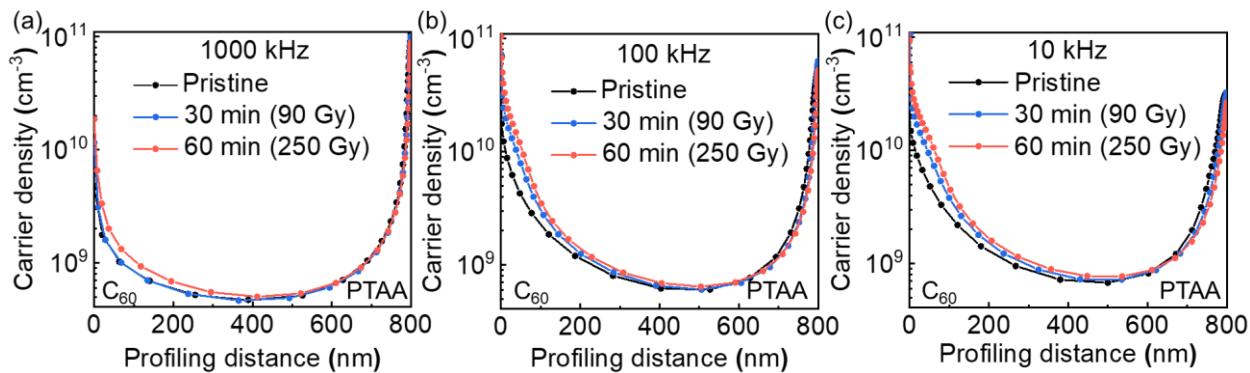


**Fig. S3.** Spatial distribution of carrier densities evolved under X-ray radiation characterized at 1000 kHz (a), 100 kHz (b), and 10 kHz (c).

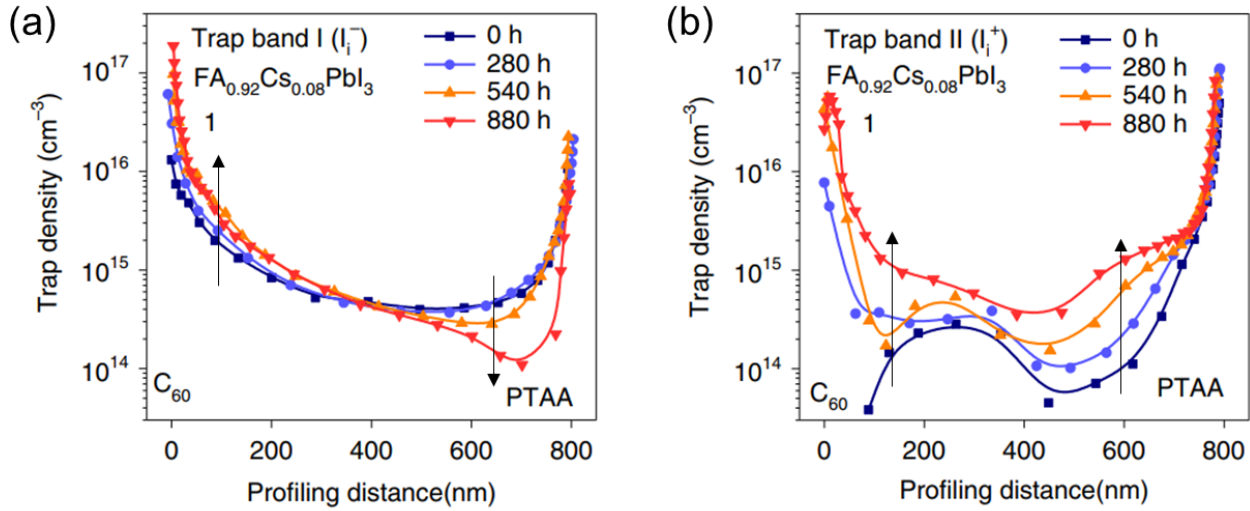


**Fig. S4.** Spatial distributions of  $\text{I}_i^-$  and  $\text{I}_i^+$  defects of PSC evolved under visible light illumination. Reproduced from ref. 24 with permission from Springer Nature, copyright 2022.

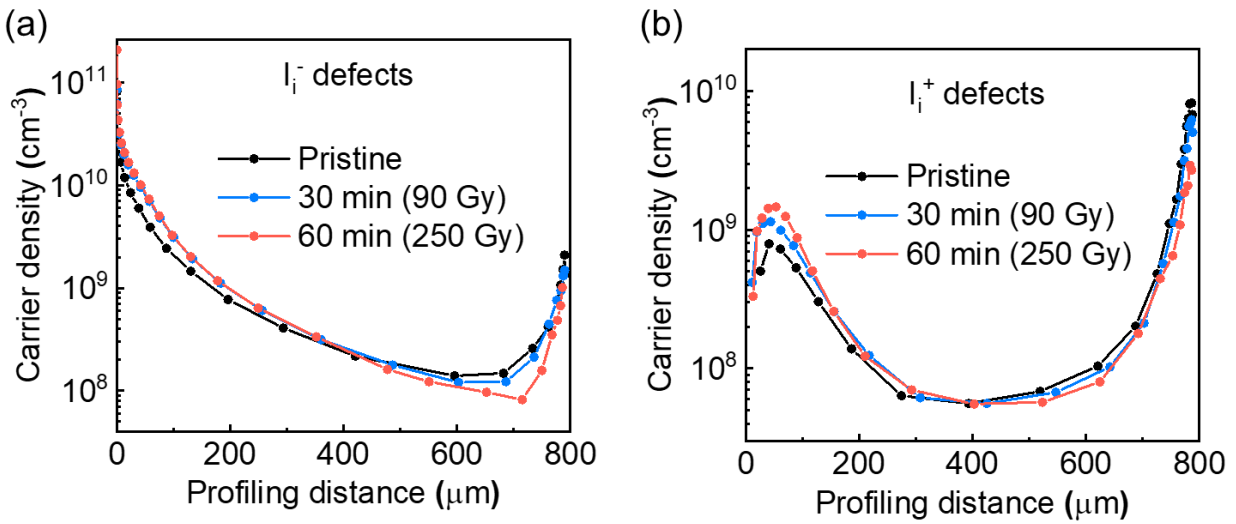


**Fig. S5.** Spatial distributions of  $\text{I}_i^-$  and  $\text{I}_i^+$  defects evolved under X-ray radiation on another perovskite solar cell.

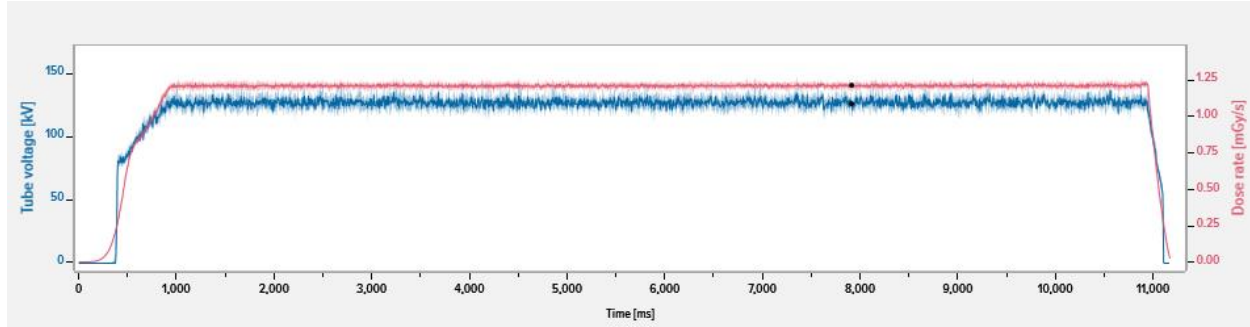


**Fig. S6.** The ramping up and damping down times of the X-ray source.

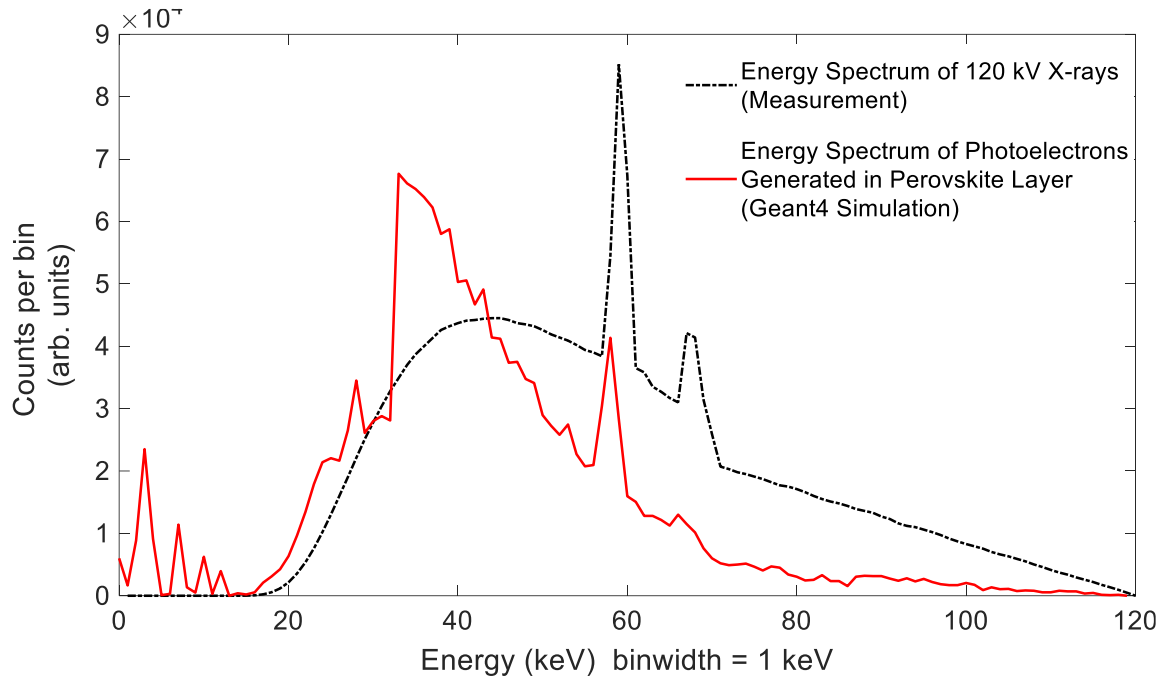


**Fig. S7.** The energy spectrum of 120 kV X-rays and the corresponding photoelectrons generated in the perovskite layer.